Modeling Soot and Its Functionalization under Atmospheric or Combustion Conditions by Density Functional Theory within Molecular (Polycyclic-Aromatic-Hydrocarbon-like) and Periodic Methodologies

Giovanni Ghigo, Andrea Maranzana, and Glauco Tonachini*

Dipartimento di Chimica Generale ed Organica Applicata, Università di Torino, Corso Massimo D'Azeglio 48, 10125 Torino, Italy

Claudio M. Zicovich-Wilson

Facultad de Ciencias, Universidad Autonoma del Estado de Morelos, Av. Universidad 1001, C. Chamilpa, 62210 Cuernavaca (MOR), Mexico

Mauro Causà*

Dipartimento di Scienze e Tecnologie Avanzate DISTA, Università del Piemonte Orientale "Amedeo Avogadro", Corso Borsalino 54, 15100 Alessandria, Italy

Received: October 7, 2003; In Final Form: November 19, 2003

Graphite, and particularly defective graphite, is chosen to model soot particles. Quantum mechanical calculations are first carried out on molecular polycyclic-aromatic-hydrocarbon-type systems and then extended to a periodic representation of one graphite layer. The features of the interaction of H, HO, NO, NO_2, and NO_3 with these model systems are examined, with the aim of defining a suitable representation of the atmospheric or combustion gas−solid interactions by which functionalization reactions can take place. The more interesting interactions with small reactive molecules regard the edge of the graphene sheet and the in-plane carbon vacancies. While these interactions can be well described by sufficiently extended molecular models, periodic models are necessary to describe accurately the equilibrium geometries because they introduce the necessary geometric constraints. The ability of a graphene sheet to easily accommodate unpaired electrons in σ or π orbitals is the basis for its interesting interactions with the small molecules present in tropospheric chemistry or combustion processes.

1. Introduction

Large quantities, ca. 13 Tg, of black carbon (soot, elemental carbon) are emitted into the troposphere during the year as a consequence of the combustion of biomass and fossil fuel. Soot aerosol contributes in a significant way to the total mass of atmospheric aerosol. It has an irregular agglomerate structure of graphene layers, and both its structure and composition can vary depending on the source.[1,2] These irregular sheets are clustered in globular particles whose dimension varies between 10 and 80 nm, approximately. In any case, a relatively large area of the particles is available for the interactions with airborne inorganic and organic molecules.

In recent times the interaction of soot with small inorganic oxidants, such as NO_2,[3−5] HNO_3,[3] H_2O,[6] and O_3,[6,7] and the oxidation of polycyclic aromatic hydrocarbons (PAHs)[5] on soot have been investigated experimentally. PAHs and their derivatives (PACs, polycyclic aromatic compounds) are ubiquitous species whose presence is widespread; beyond being produced from a variety of combustion sources, they are known as primary and secondary tropospheric pollutants, especially in urban areas.[1] This means that oxidation can either take place already during combustion or occur at a later time, during the tropospheric transport of combustion-generated particulates. Because PAHs and PACs are generated in the same combustion processes at low O_2 concentrations that bring about the more or less disordered growing of the mentioned graphite-like layers, they share the same nature of soot.[1,2] Because of the origin and structural affinities, they are often found to be associated with the carbonaceous particulate (because PACs have been detected in diesel exhaust, they have also been supposed to possibly originate on the surface of particulate matter).[8]

The functionalization of PAHs and of soot itself has been studied by both field campaigns and laboratory studies.[9] While being transported, different PAHs decay at very different rates. Then, the relative amounts of carcinogenic/mutagenic primary products change significantly and other products form whose nature is in some cases known and in others is not.[10] Therefore, the transformation of primary pollutants, either through gas-phase reactions or by heterogeneous processes (via their interaction with the fine particulate), is of great interest from chemical and toxicologic points of view. One important aspect is that as the compound or particle polarity increases, so does its water solubility, and it can be more easily brought by the aerosol into contact, for instance, with the lung tissues. Therefore, PAHs and PACs adsorbed on fine particles are of concern as regards human health.

In addition, it would be important not only to get a more precise picture of the ambient levels of both the primary and

* To whom correspondence should be addressed. For G.T.: (e-mail) glauco.tonachini@unito.it; (fax) ++39-011-6707642; (Web site) www.thecream.unito.it. For M.C.: (e-mail) causa@al.unipmn.it; (fax) ++39-0131-287416.

10.1021/jp037011+ CCC: $27.50
Published on Web 02/12/2004

the secondary PAC productions but also to achieve a better knowledge of the structural features and transformation mechanisms of primary and secondary PAC pollutants. In this respect, the PAH and soot functionalizations could share some mechanistic features. The functionalization mode poses some problems. Because the oxidative pathways leading from PAHs to PACs, or to soot functionalization, can be obviously characterized not only by the intervention of monomolecular steps but also by involvement of other species such as HO, NO, NO_2, and O_2 (present in variable concentrations), different environmental or combustion conditions can modulate the relative importance of possibly competing pathways.[11−17] Finally, it can be remarked that oxidation processes of PAHs produce a variety of compounds, which have been only partially identified.[14]

Investigating the nature of the interaction of small inorganic oxidants with the surface of soot particles by theoretical means could be instrumental for a better understanding of some aspects of combustion and tropospheric processes and can be seen as complementary to the valuable data collected experimentally. The present study is undertaken first by defining a suitable model for soot and then by modeling some selected functionalization (especially oxidation) processes. Quantum mechanical calculations are first carried out on molecular PAH-type systems. These are actually gas-phase reactions, such as those already examined in this laboratory,[18] which are expected in this case to be instrumental in setting up a model. The computations are then further extended to a periodic representation of a (undefective or defective) graphene layer, which is chosen to model soot particles. In this respect, some recent work along the same line can be mentioned.[19−21] Then, our goal is to define a suitable model for the gas−solid interaction by which functionalization reactions can take place. So the features of the interaction (possibly chemisorption) of some small species (H, NO, NO_2, and NO_3) are examined. The lack of structural information on the atomic scale about soot and its possibly active surface sites (useful to set up a computational study and for subsequent comparative purposes) constitutes one problem. Only a few experimental studies report on this issue to some extent.[7,22] Both the molecular and the periodic models considered here are in principle dimensionally inadequate for opposite reasons: soot is made up by finite graphene layers larger than our PAH molecular models, yet not stretching out infinitely in two dimensions, as most of our periodic models do. However, if these two extreme models give consistent, not conflicting, answers about the local chemical behavior, they will probably describe correctly local chemical features of soot particles. A further development, beyond the scope of this initial study, will aim to elucidate if soot can have a role in setting the scenario for possible functionalization channels of aromatic compounds.

2. Methods

The stable and transition structures were determined by gradient procedures[23] within the density functional theory (DFT) and by making use of the B3LYP functional.[24] The same functional has been used in molecular and periodic calculations. This functional is of widespread use, and, even if prone to underestimate some reaction barriers, has generally performed well as regards geometries and energetics.[25] The unrestricted spin density functional theory has been applied to spin-polarized models, both molecular and periodic calculations. The polarized 6-21G(d) basis set[26] was used in the DFT (B3LYP) optimizations. The 6-21G basis set is preferable than the most popular 6-31G basis set in periodic LCAO calculations. To avoid numerical consequences due to a badly defined exchange potential or the quasilinear dependence of basis functions,[27] especially for nearly conductive materials such as graphite, the value of the external valence coefficient for carbon is increased from 0.197 to 0.240. This modification would be dangerous for the 6-31G basis set, where the three sp exponential coefficients of the internal valence linear combination are 7.87, 1.88, and 0.54: the 0.54 and the 0.24 Gaussian exponents are too close, and this could lead to numerical instabilities. On the other hand, this problem is absent with the 6-21G basis set, where the exponential coefficients of the two internal valence Gaussians are 3.66 and 0.77. A complete set of critical-point geometries and energies is presented, together with the relevant spin densities, when appropriate, in the Supporting Information, section 1 (molecular computations) and section 2 (periodic computations). All molecular calculations were carried out by using the Gaussian 98 system of programs.[28]

The periodic LCAO calculations were performed using the CRYSTAL program;[29] structures periodic in three (bulk crystals), two (slabs), and one dimensions (polymers) can be treated by using Hartree−Fock, density functional, and hybrid Hamiltonians. The periodicity is fully considered by using cyclic boundary conditions; the infinite series of Coulombic integrals is approximated by Ewald techniques,[30] while the infinite exchange series, representing an essentially short-range interaction, is truncated ensuring convergency on energy and related observables.[31] The solution of the effective one-electron Schroedinger equations is performed in the reciprocal space. The k-points are sampled on a regular mesh; for conducting systems, the Fermi surface is calculated using a denser K-point mesh, using Fourier interpolation of energy bands.[27] The symmetry is fully implemented in the direct space, for minimizing the number of molecular integrals to compute and to store, and in the reciprocal space, for performing a block-diagonalization.[32] Recently, energy derivatives with respect to the position of the atoms in the unit cell have been implemented in Crystal.[33] Therefore, it is possible to carry out an automatic optimization of the equilibrium geometry within a given crystal symmetry.

Surface defects, adsorption, and adsorption on defects is studied by two-dimension periodic super-cells. The substrate is represented by a number of atomic layers. The convergence of the surface properties versus the number of atomic layers is normally fast because of the exponential decay of the surface electrostatic field orthogonal to the surface. The convergence is moderately fast with ionic surfaces[34] and slower with metallic and covalent surfaces, because of the propagation of the effects of the surface dangling bonds. In the case of the graphite, the covalent graphene layers are bound by the dispersion forces, which are not properly taken into account by Hartree−Fock or DFT methods.[35] The neighbor layer only weakly influences the electronic structure, as can be shown by theoretical and experimental studies of graphite scanning tunneling microscope images.[19] On the other hand, a single graphene layer can describe the surface chemical properties of graphite. We calculated, as reported below, hydrogen adsorption on graphite using one and two layers, obtaining about the same interaction energies, within the estimated error of periodic calculations of this type, that is, about 1.5 kcal mol^{-1}.

3. Results and Discussion

The simplest radical for which the interaction with a graphene layer was considered is the hydrogen atom. Though simple, the H radical is quite important in hydrocarbon combustion processes, giving origin to soot in the case of incomplete combustion. This is because it enters the main propagation (and

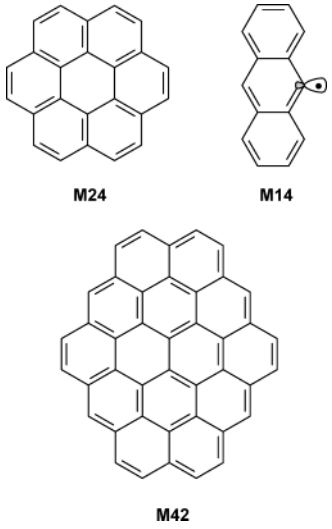

Figure 1. PAH molecular models adopted in the study.

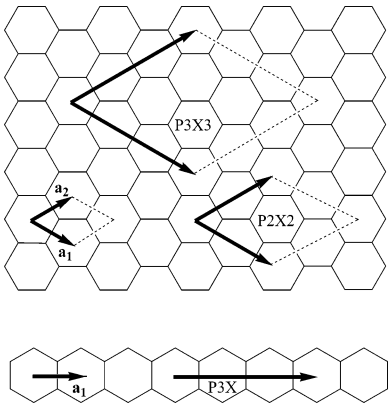

Figure 2. Periodic models: (top) two-dimensional unit cell and supercells ($\mathbf{a}_1$ and $\mathbf{a}_2$ are the fundamental lattice vectors); (bottom) one-dimensional unit cell and supercell.

chain branching) steps, as well as the main termination step. These are the reaction steps that affect in a major way the overall radical concentration and hence the reaction rate.[36] In this respect, it is interesting to assess if the interaction of H with soot is so effective to quench its activity to some extent or, conversely, if other important species, as OH, also involved in propagation steps of the combustion processes, can interact in such a way with soot to release H. These aspects were addressed as regards the interaction with molecular and periodic models of a nondefective or defective graphene layer.

3.1. Comparison of Molecular and Periodic Models. The molecular and periodic models have been initially compared, as regards the hydrogen "on-top" adsorption (i.e. with H located above one carbon and perpendicularly to the plane defined by the three adjacent carbons C′) on a nondefective graphite layer.

The two molecular models, i.e., the PAHs M24 ($C_{24}H_{12}$) and M42 ($C_{42}H_{16}$), are displayed in Figure 1. They have an even number of carbon and hydrogen atoms to keep the same spin multiplicity of the periodic models (i.e., singlet, without H adsorbate). The periodic models are single layers of hexagonal graphite, with cyclic boundary conditions in two dimensions. Supercells P2X2 and P3X3 have been analyzed, as reported in the Figure 2.

Because the graphite layers are weakly bound by van der Waals forces (for which density functional models cannot described correctly),[35] we had to ascertain if a model constituted by a single layer was adequate. A second graphene layer comes out to insignificantly affect the surface chemical properties and only weakly affect the surface density.[19] To further confirm that using a single graphene layer is adequate, we calculated the hydrogen adsorption energy in the presence of one or two layers, held at the experimental distance for graphite, 3.35 Å. One and two layer models give the same adsorption energy for the P3X3 model; we calculated respectively −18.7 and −17.3 kcal mol^{-1} for single and double layer of atoms. These results can be considered in good agreement. The lower adsorption energy on the double layer model is due to fact that we adopt the geometry optimized for the single layer model. On the other hand the difference between the adsorption energies using one and two graphene layers, about 1.5 kcal/mol, gives an upper limit to the error that we introduce using a single graphene layer, as we do in all our studies.

TABLE 1: Comparison of Molecular and Periodic Models[a] Showing Adsorption Energy[b] of One Hydrogen Atom on Small PAHs and Graphite

model	ΔE	model	ΔE
M24	−12.1	P2X2	−17.1
M42	−16.9	P3X3	−18.7

[a] M*n* are small PAH systems made by an even number *n* of carbon atoms defined in Figure 1. P*m*X*m* are periodic models defined in Figure 2, consisting of *m*X*m* supercells. [b] In kcal mol^{-1}.

Only one energy minimum is detected for both molecular and periodic models, corresponding to the mentioned "on-top" situation, in which the H atom interacts with one carbon perpendicularly to the plane defined by the three adjacent carbons C′.[37] This is a moderately perturbed situation, especially as regards the energy effects. In fact, the absorption energy is in the range of the low-energy chemisorption. However, the geometry is locally quite different from the planar sp^2 situation of graphite and approaches the geometry of a tetrahedral sp^3 carbon. The C(∼sp^3)−H distance is 1.13 and 1.15 Å in the molecular M42 and periodic P3X3 models, respectively. The HC(∼sp^3)C′ angle is 114° and 113°. The spin densities on H and C atoms are below 0.1 electron in both models. The spin densities on the C′ atoms are higher in the P3X3 model (0.28 electron) than in the M42 model (0.12 electron).

The adsorption energies are reported in Table 1. The molecular models indicate a binding energy in the range 12−17 kcal mol^{-1}, while the periodic models span the range 17−19 kcal mol^{-1}. The physical description produced by the two classes of models are clearly the same; the graphene sheet establishes a weak chemical bond with the H radical. The range of binding energies of the molecular models shows the importance of the cluster truncation. The data in Table 1 indicate that the description of the H−surface interaction afforded by either molecular or periodic calculations is the same and suggest that a molecular model of sufficient size is apt to describe the existing effects.

The M42 molecular model (Figure 1) and the P3X3 supercell (Figure 2) have been chosen for further studies, on the basis of the molecular and periodic adsorption energies for hydrogen. M42 is computationally treatable, and the P3X3 supercell, which includes 18 carbon atoms in the unit cell, provides an acceptable convergence of the electronic structure, a condition necessary to perform an automatic geometrical optimization. With M42, the closest distance of the H adsorbate from the border atoms is 5.0 Å, corresponding to the fourth nearest neighbor in the graphite structure. The closest distance between the H adsorbates in the P3X3 supercell is 7.4 Å, corresponding to the sixth nearest neighbor. In both cases this distances appears to ensure, for relatively small adsorbates, a reasonable chemical environment.

TABLE 2: Adsorption Energies[a] of Some Small Molecules on the M42 PAH Model and on a Graphite Sheet

model	M42	P3X3
H	−16.9	−18.7
OH	−16.7	−15.2
$^3O_2$	−0.8	−2.8
NO_2 (O side)	22.9	26.0
NO_2 (N side)	−1.7	−4.0
NO_3	−1.5	−4.0

[a] In kcal mol^{-1}.

The M42 and P3X3 optimal geometries are very similar: the C−H distance is 1.13 and 1.15 Å, respectively, the C−C′ distances are 1.51 Å in both cases, and the pyramidalization angle HCC′ is 104° and 106°, respectively. The C−H and C−C′ distances can be compared to the corresponding bond lengths for small molecular radicals, calculated at the same computational level (B3LYP/6-21G(d)). The C−H distances are in the range 1.10−1.11 Å for more ordinary hydrocarbon radicals, as CH_3CH_2, $(CH_3)_2CH$, and $(CH_3)_3C$, while the C−C distances are in the range 1.48−1.49 Å. The longer bond distances found in our molecular and periodic models of hydrogen radical adsorption on graphite are due to a more stressed equilibrium geometry because the sp^2−sp^3 rehybridization cannot fully take place, as demonstrated by the HCC′ angles. For the same reason, the C−H bond length on graphite is longer than the C−H distances computed (though at different computational levels) for hydrogenated fullerenes: 1.10 Å $C_{28}H_4$[38] and 1.08 Å for $C_{60}H_{12}$,[39] because in these systems a higher degree of pyramidalization than in graphite can be reached.

The spin density P from the Mulliken population ($P = P^\alpha - P^\beta$, excess α electron population over β) can be used as a useful tool in electronic structure analysis when the same basis set and Hamiltonian are employed. The features of P show that the unpaired electron (originally on H) gets spread around; while P on the interacting hydrogen and the underlying carbon is negligible, a P value of 0.11 e (M42) or 0.28 e (P3X3) is found on the three nearest neighbor C′ atoms. All the other spin populations are smaller, with the exception of some of the border carbon atoms of the molecular models. So the unpaired electron is delocalized on the π orbitals of the graphite and is slightly more removed from the adsorbate zone in the molecular model than in the periodic model, in which this is not allowed by the presence of the neighbor adsorbed groups. A common feature of molecular and periodic spin-polarized calculations is the appearance of spin waves; the spin density positive values alternate with negative values, which are lower in absolute value. The amplitude of spin waves does not decrease with the increasing dimensions of the molecular model or, in the periodic model, of the cell. As a consequence, large PAH-like systems with one unpaired electron show several atomic spin density population with significant values, around 0.2 electron.

3.2. Adsorption on Graphite. Table 2 shows the adsorption energies of some small radical molecules on graphite, obtained with the M42 and P3X3 models in correspondence to optimized geometries. Only H and OH show on-top chemisorption, while the structures characterized for O_2, NO_2, and NO_3 are not bound from the point of view of energy, geometry, or both. O_2, NO_2 (interacting with the N atom), and NO_3 form intermolecular complexes with graphite at distances of ca. 3 Å. NO_2, if adsorbed at closer distance by engaging the O side, shows an endoergic minimum of the potential energy surface. OH, as the H atom, causes a pyramidalization of the underlying graphitic carbon (Figure 3). The C−C′ bonds are elongated to some extent with respect to their values in the unperturbed models: 1.51 Å in M42 (vs 1.41 and 1.43 Å) and 1.49 Å for P3X3 (vs 1.43 Å). The C−O bond is 1.48 Å for M42, and 1.53 Å for P3X3, which is somewhat longer than a typical single C−O bond. OH is slightly less bound in the periodic model (Table 2).

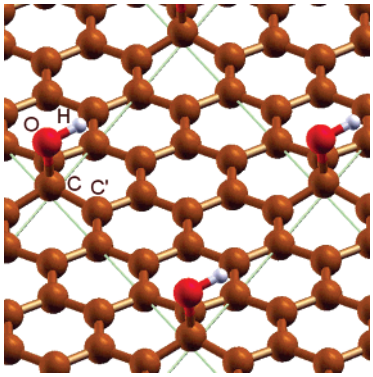

Figure 3. OH adsorption on P3X3 periodic model. A total of 1 out of 18 carbon atom is bound to OH. Atom C, directly bound to OH, has partial sp^3 character. The O−C−C′ angle is 115°, the C−O distance is 1.57 Å, and the C−C′ distance is 1.49 Å. The unpaired electron is delocalized. The residual Mulliken spin population of OH is 0.11 e. C has a spin population of −0.05 e, while each first neighbor C′ has 0.25 e.

The spin density on OH is negligible and is found again to be highly delocalized on the PAH or graphitic system. The NO_2 molecule, when adsorbed by involving one O atom, turns out to be very distorted. The ONO angle changes fom 134° in NO_2 to 109° for adsorbed ONO. The external O−N bond length is 1.20 Å, but the internal one is 1.44 Å. This is to be compared with the O−N bond length in the free molecule, 1.21 Å. The local pyramidalization of the surface is roughly the same as in the OH adsorption. The C−O bond is 1.54 Å, indicating the formation of a real bond with the underlying carbon on the surface. The concomitant N−O bond stretch costs about 30 kcal mol^{-1}, as we estimated by comparing the NO_2 molecule itself either optimized or in the geometry relevant to the adsorbate situation. The local endoergic minimum has a small barrier of 1.6 kcal mol^{-1} for the dissociation of the NO_2 molecule from the surface. NO_2 shows a low reactivity with respect to unsaturated molecules; the reaction energy with ethene, at the same computational level, is 2.0 kcal mol^{-1} from the N side and is −0.6 from the O side. The direct attacks of NO_2 to naphthalene and benzene, which could be compared to the present case, are addressed in another paper[40] and come out to be very unlikely, requiring ca. 25 or 30 kcal mol^{-1}, respectively.

We conclude that only very reactive radicals, such as H and OH, are able to strongly interact with the π electronic system of the graphite surface and become chemisorbed. Of them, hydroxyl is an important species both in the atmospheric chemistry and in hydrocarbon combustion. Hydrogen plays an important role in the latter.

3.3. Carbon Vacancy on the Plane. The simplest graphite defect is a one-atom vacancy. A defect of this kind (a hole on the surface) was indeed detected by scanning tunneling microscopy,[41] but only in the case of a deficiency of several atoms. In that case, an internal edge of the layer is formed whose geometric and electronic structure features are common to the external edge. The two situations are in fact indistinguishable in the limit of a large hole. We will consider first the simple case of a single atom vacancy, and in a subsequent section we will consider that of a sheet edge.

The formation energy for the one-atom hole defect is the cost of getting this atom from the surface to infinite separation. This

TABLE 3: Formation Energy of Carbon Vacancy[a] for Molecular and Periodic Models[b]

model	singlet	triplet
M24	328.8	309.5
M42	365.8	334.5
P2X2	351.7	342.5
P3X3	383.4	365.1

[a] In kcal mol^{-1}, computed as the difference between the energy of the defective model plus one carbon atom at infinite distance and the energy of the undefective site. [b] The results of the periodic models are given at periodic optimized geometries.

CHART 1

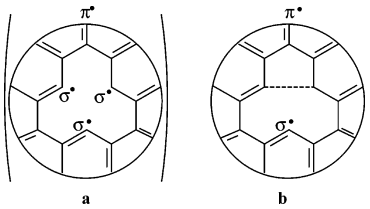

energy, as assessed within two molecular and two periodic models, is reported in Table 3. As regards the spin multiplicity of the hole containing system, the triplet is indicated as stabler than the singlet by both molecular and periodic models (Chart 1a).

The formation energy of the defect is roughly equivalent to the energy of three graphite bonds. This energy increases, in both the molecular and periodic cases, as the dimension of the model increases. This is probably due to the stiffer geometric constraints that the increasing number of surrounding rings imposes to the hole zone. Actually, the original trigonal symmetry is broken upon defect formation, since two of the three atoms carrying an unpaired electron (see Chart 1b) spin-couple their electrons to try to make a single bond, and a five membered ring is consequently formed. This geometrical feature is evident in both models, though more pronounced in the molecular one. The C2−C3 interatomic distance is 1.74 Å in the M42 model (Figure 4) and 2.13 Å in the P3X3 model (Figure 5). Although the DFT approach is not the most reliable in such a stretched situation, the $\langle S^2 \rangle$ value indicates little contamination by the higher spin multiplicities, being 2.0735. If a quintet, endowed with a local triplet nature as regards C2 and C3, were involved, it could actually be at the origin of the significant stretching reported. However, an explicit calculation on the quintet for C42 produces a different description characterized by a decoupling of the spin of π electrons and not of those associated with the C2 and C3 lobes. Moreover, this quintet is 47.6 kcal mol^{-1} above the triplet. Therefore, on the basis of the $\langle S^2 \rangle$ value and the energy, we are inclined to attribute the stretching to the rigidity of the system.

The residual spin density on the two interacting carbons is small: 0.09 and 0.34 electron in M42 and in P3X3 models, respectively. In the molecular M42 model the residual spin population can be attributed totally to pπ orbitals. By contrast, a σ dangling bond is localized on the third atom around the vacancy, and its Mulliken spin density is ca. 1 electron. The presence of the σ dangling bond and the five-membered ring around the vacancy does not bring about any significant deviation from planarity in both the periodic and molecular models. The π spin density is largely delocalized, as found in the case of the OH adsorption on undefective graphite.

3.4. Adsorption on the In-Plane Vacancy The in-plane vacancy is very reactive, and small radicals are bound with strong adsorption energy (see Table 4). The most stable spin

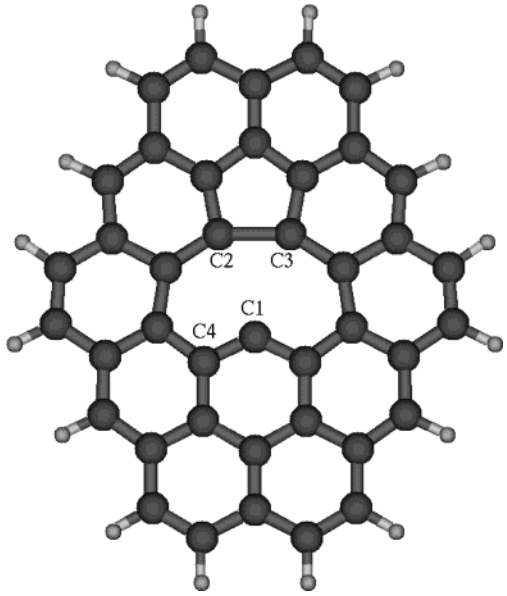

Figure 4. In-plane carbon vacancy as described by the molecular model C42. The C2−C3 distance is 1.74 Å, which is compared to the normal second neighbor distance of 2.46 Å. The C1−C4 distance is 1.35 Å. The most stable spin state is a triplet. One electron is localized in a σ dangling bond of atom C1, which has a Mulliken spin population of 1.16 e, while the second electron is delocalized in the π orbital.

state has been considered, that is, doublet for all the adsorbates but for O_2, which is triplet. The molecular and periodic models give the same qualitative description, yet they produce slightly different quantitative results. The adsorption energies on M42 are systematically higher, because the cluster can modify its geometry to better accommodate the molecule, with respect to the stiffer periodic model. It is interesting that NO_3 and NO_2 (with one oxygen interacting with the radical center) are adsorbed in a dissociative way. This means that as an oxygen atom becomes bound to the σ vacant site with formation of a carbonyl group, NO_2 and NO are concurrently released. These events correspond to a concerted process. On the other hand, NO_2 forms quite a strong bond with the in-plane vacancy if nitrogen interacts with the radical center, and the C−N bond distance is 1.45 Å in the M42 model.

The formation of a carbonyl group upon interaction of an oxygen atom with the vacant site is such a favorable chemical event that can also occur upon OH adsorption onto this radical center. In fact, in the case of hydroxyl the undissociative (Figure 6a) and H−O dissociative (Figure 6b) adsorptions have about the same energy (Table 4). In the latter, the hydroxyl H atom becomes bound to a carbon belonging to the five-membered ring. If, by contrast, the carbonyl group were formed by concurrently leaving a free H atom, this situation would be 46 kcal mol^{-1} above the M42-OH adduct. In the H-bound dissociative case, the C−H bond length is almost normal, 1.11 Å, and this is obtained at the expense of the adjacent carbon−carbon π bonds of the 6-ring, which get stretched significantly: C3−C4 from 1.486 to 1.589 Å; C3−C5 from 1.431 to 1.507 Å (C2−C3 is less affected, going from 1.682 to 1.741 Å). In fact, this H migration from O to C should be quite easy not only because the process is isoergic but also because the hydrogen is already rather close to the C3 and C4 atoms in the initial adduct (2.278 and 2.280 Å, respectively). The possible migration of this hydrogen on the surface is presently under investigation but seems rather difficult, on the grounds of preliminary tests. Thus, the adsorption of radicals on graphenes with this kind of highly reactive defect appears to have basically

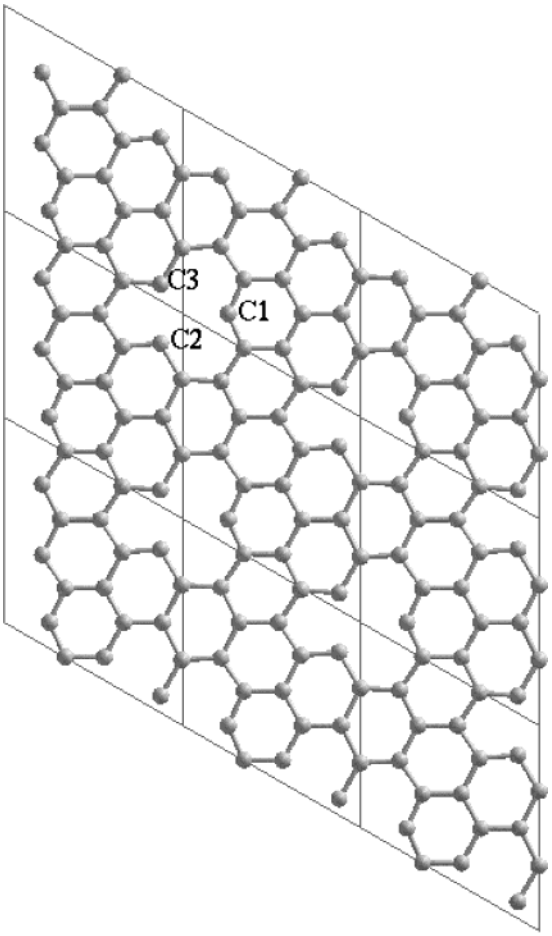

Figure 5. In-plane carbon vacancy as described by the periodic model P3X3. Nine unit cells are represented to show the defect density. The trigonal symmetry is lost as in the molecular model, but the geometry relaxations are less pronounced. The C2−C3 distance is 2.13 Å, while C1−C3 and C1−C2 distances are 2.65 Å. Again, one unpaired electron is localized in the C1 σ dangling bond (the spin density population is 1.12 e), and the other unpaired electron is delocalized in the π crystalline orbitals.

TABLE 4: Adsorption Energies[a] of Some Small Molecules on the Vacancy[b]

model	M42	P3X3	type of adsorption or bonding
H	−104.9	−95.9	bound
OH	−107.9	−91.8	bound
	−107.7		dissociative
$^3O_2$	−48.1	−22.2	bound
NO_2 (O side)	−80.6	−57.8	carbonyl group + NO
NO_2 (N side)	−52.6	−30.7	bound
NO_3	−105.1	−78.7	carbonyl group + NO_2

[a] In kcal mol^{-1}. [b] The interactions between the adsorbed molecules are below 0.5 kcal mol^{-1}.

local consequences. The bond formation is irreversible at room temperature and thus can be hardly connected with any catalytic process. However, these soot functionalizations by radicals, with carbonyl formation, have interesting propagation aspects because they in turn release other free radicals (NO_2, NO, and H).

The geometries obtained by adsorption within the P3X3 periodic and the M42 molecular models are significantly different. In fact, the presence of the periodic boundary condition does not allow the system to relax to better accommodate the adsorbed molecule, as the molecular model can do. As an example, in the case of the dissociative NO_2 adsorption, the angle of the C═O double bond with the opposite carbon atom

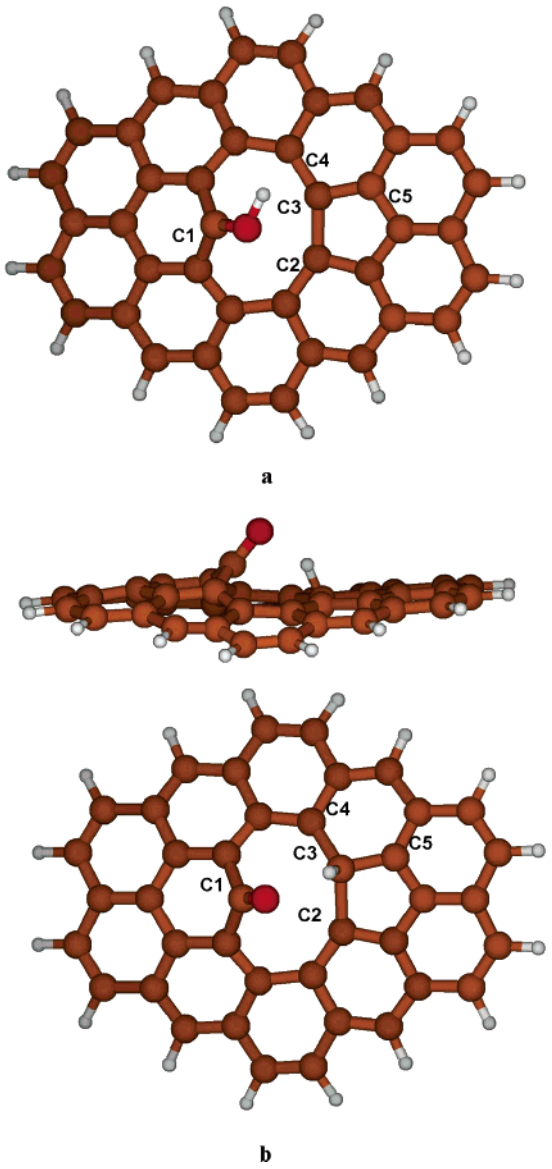

Figure 6. OH adsorption on the in-plane vacancy as described by the molecular M42 model: (a) nondissociative HO adsorption; (b) dissociative adsorption, side view and top view (the C═O bond length is 1.23 Å, typical of a double CO bond). The unpaired electron is delocalized.

(see Figure 6b) is 65° for the M42 model and 78° for the P3X3 periodic model. For these geometrical reasons the adsorption energies for the P3X3 periodic supercell are lower, even if they indicate again an irreversible adsorption.

Because we like to begin probing the potential capability of graphene defects to activate some reactions involving aromatic hydrocarbons, we have chosen here the hydrogen abstraction from benzene by the hole vacancy as a first preliminary and simple case (the same process, but taking place on the edge vacancy, is discussed below). Table 5 reports the energetics for this reaction.

The barrier has been calculated by using the Gaussian 98 transition structure search algorithms. The correspondence of the imaginary frequency to the expected reaction coordinate has been checked for the molecular models M14 and M24. The molecular geometries of the transition structures have been then transferred to the periodic P3X and P3X3 models, and a partial geometrical optimization has been performed, keeping the C−H distances at the values of the molecular transition structures.

TABLE 5: Energies[a] of Hydrogen Abstraction from Benzene by In-Plane and Edge Vacancies

	In-Plane Vacancy	
	M42	P3X3
barrier	16.6	32.4
reaction energy	13.2	22.2
	Edge Vacancy	
	M14	P3X
barrier	4.6	3.8
reaction energy	0.1	2.6

[a] In kcal mol^{-1}.

The intermediates produced by this process are a phenyl radical plus the model (M42 or P3X3) having its vacant site saturated by the abstracted H. Though the "reactants" and "products" look at first sight rather similar, the reaction is considerably endoergic and the H-abstraction barrier is quite high. The periodic model shows a higher energy and barrier for the "in-plane" situation because of the relaxation difficulties and a small lateral interaction between the benzene molecules in the P3X3 supercell (this term is estimated to correspond to 1.5 kcal mol^{-1} per cell). However, though the radical site in the molecular model presents a lower barrier, it hardly performs the H abstraction. This can be at least in part attributed to the modest hole size that forces unfavorable geometric approaches. Enlarging the hole could change the outcome, but a hole large enough to allow it to proceed by a collinear process would obviously shade off into a defective border situation. This is indeed the next case we have examined.

3.5. Adsorption on the Edge Vacancy. Modeling the mechanism of carbonization and graphitization, as formulated by some authors,[42] involves the intervention of polycyclic aromatic species with unsaturated carbons on the border[43] (σ radical sites). Some models[21] have been built by assuming the presence of several adjacent σ dangling bonds, a situation that seems to us somewhat strained. On the other hand, convincing experimental information about the number and the nature of the radical sites is not abundant. Therefore, we prefer to explore the characteristics of a single σ dangling bond, located on a sheet border, to which we also refer as "edge vacancy".

Again, molecular and periodic models are employed to study the edge vacancy. On the basis of the study by Cioslowski et al.,[44] in which the C−H bond energies in benzene and other nine PAHs are 106.7−107.6 kcal mol^{-1}, the chosen molecular model is simply the 9-anthranyl ($C_{14}H_9$) radical (Figure 1), labeled M14 for short. The "one-dimensional" (tape) periodic structure adopted to represent a graphene sheet edge is an infinite polyacene tape.

This choice was put to the test by comparing the electronic structure of this linear periodic structure with that of the two-dimensional periodic model already used to represent one graphene layer. The valence band structure and density of states of the latter are plotted in Figure 7, while the same observables for the polyacene model are plotted in Figure 8. The contribution to the density of states coming from the hydrogen atomic orbitals was projected out. A comparison of the two figures suggests that the graphite electronic structure is well reproduced by the polyacene system. Both are semimetal; the quasi-degeneracy between the highest occupied and lowest unoccupied crystalline orbitals (HOMO and LUMO) at the border of the first Brillouin zone gives a minimum in the density of states at the Fermi level.

The shape and energy range of the density of states are almost the same in the one- and two-dimensional models, even if the

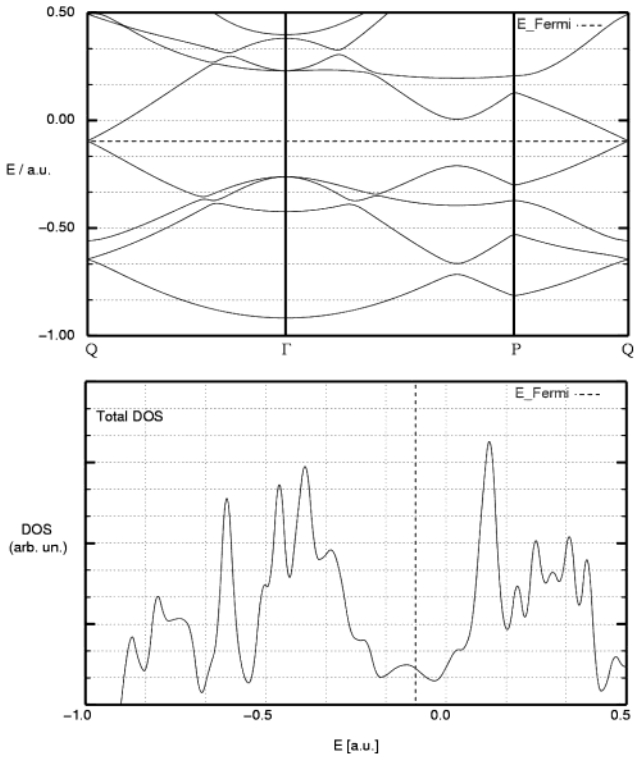

Figure 7. Band structure (top) and density of states (bottom) of graphite, as calculated by periodic model, using the primitive unit cell. Only the valence and the first conduction bands are reported. The highest energy crystalline orbitals (HOMO) and lowest unoccupied (LUMO) have π character.

1D model has a nonzero energy gap, as discussed in the literature.[45] This very small energy gap, about 0.2 eV, cannot influence the chemical property and the reactivity of the models. The C−H bonds are embedded in the middle of the valence and the conduction bands, and consequently do not contribute to the HOMO and LUMO, made only by the carbon pπ orbitals. The C−H σ bonds, which are the most interesting chemical feature of the edge, are localized in a different energy range with respect to the π delocalized crystalline orbitals. On the basis of this analysis, we can conclude that the polyacene system reproduces well the electronic structure features of a graphene sheet, as regards the reactivity.

To avoid a potentially disturbing crowding of radical sites (with possible interactions and consequences as regards the definition of the spin multiplicity), a triple supercell was utilized, referred to as P3X (Figure 2). Table 6 reports the binding energies relevant to the usual set of small radical species and the edge vacancy, as determined within the molecular and periodic models. The first line (H) is also the formation energy of the vacancy. The two sets of values, for the M14 and P3X models, are rather close. The radical molecules get adsorbed quite strongly and irreversibly to the edge vacancy (actually they become covalently bound to it). Soot functionalization by this kind of process appears rather easy.

We extended to the edge vacancy the exploration of the capability of activating an aromatic molecule toward functionalization by hydrogen abstraction. The last two lines in Table 5 report the reaction energy and energy barrier of the M14 and P3X models of edge vacancy reacting with benzene (Figure 9). The reaction is almost isoergic because the C−H bond energy is very similar in the reactants and in the products.[44] The energy barrier is also very small, about 4 kcal mol^{-1}, because of the favorable collinear geometry that gives optimum orbital overlap

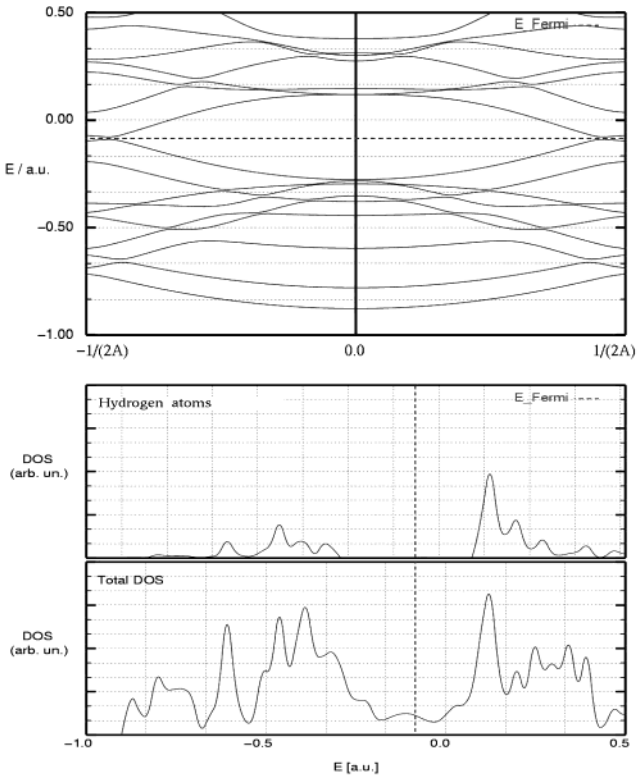

Figure 8. Band structure (top) and density of states (bottom) of one-dimensional periodic model of an infinite polyacene as a model of a graphene edge. The main features of the graphite band structure, as reported for comparison in Figure 8, are reproduced. The hydrogen atoms do not contribute to HOMO and LUMO crystalline orbitals, which have π character, because their projected density of states, reported in the upper part of the DOS, are relevant only in the middle of the valence and conduction bands.

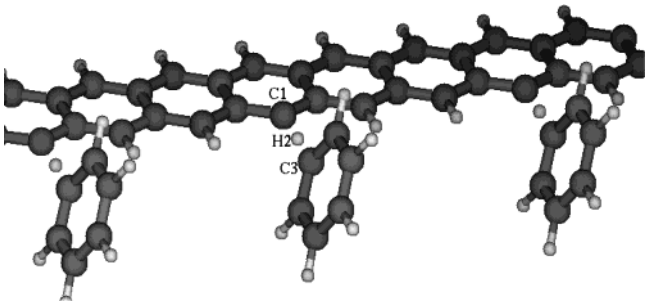

Figure 9. Transition structure for H abstraction from benzene by the edge vacancy, as described by the P3X periodic model. Both C1−H2 and C3−H2 distances are 1.34 Å.

TABLE 6: Adsorption[a] Energies for Molecular (Anthranyl) and Periodic (Polyacene) Models[b]

model	M14	P3X
H	−118.0	−115.5
OH	−121.8	−116.2
$^3O_2$	−55.7	−59.5
NO_2 (O side)	−81.7	−74.4
NO_2 (N side)	−72.7	−67.5
NO_3	−106.8	−98.8

[a] In kcal mol^{-1}. [b] The periodic results are obtained at the optimized molecular geometries.

for the H transfer. On this basis, we can conclude that the edge vacancy is a more interesting site that can participate in radical reactions of various molecules interest, both as a propagator and as a terminator of radical chain reactions.

4. Conclusions

Possible periodic and molecular models of reactive events taking place on the surface of a graphene have been defined. The genuine solid-state effect, which in principle can be treated only with periodic models, regards only the π system of electrons, while the more interesting interactions with small reactive molecules regard σ orbitals, both at the edge of a graphene layer and at carbon vacancies (holes) within the sheet. The interaction with σ orbitals are more localized and can be described well with molecular models. The ability of delocalizing π unpaired electrons can be reproduced with molecular models of sufficient dimension, such as M24 and M42, that take into account all the electronic features accurately. Periodic models are necessary, on the other hand, to correctly describe the equilibrium geometries because they introduce the required geometric constraints, while the molecular models allow a larger geometrical freedom. This preliminary study shows that the most interesting possible interactions of a graphite-like model with the small molecules present in tropospheric chemistry or combustion processes are based on the ability of easily accommodating unpaired electrons and their possible presence in σ and π orbitals. This point will be the subject of further theoretical study, which we will perform on the basis of the P3X3 supercell and the M42 molecular model for surface events, and the M14 molecular model and P3X periodic for edge events.

Acknowledgment. Funding by the Italian CNR (Agenzia 2000) is gratefully acknowledged.

Supporting Information Available: Geometries of all optimized structures, the corresponding total energies, and further information about atomic spin densities. This material is available free of charge via the Internet at http://pubs.acs.org.

References and Notes

(1) Finlayson-Pitts, B. J.; Pitts, J. N., Jr. *Chemistry of the Upper and Lower Atmosphere*; Academic Press: New York, 2000; Chapter 10, Sections E and F.

(2) Homann, K.-H. *Angew. Chem., Int. Ed.* **1998**, *37*, 2434−2451.

(3) Kirchner, U.; Scheer, V.; Vogt, R. *J. Phys. Chem. A* **2000**, *104*, 8908−8915.

(4) Arens, F.; Gutzwiller, L.; Baltensperger, U.; Gäggeler, H. W.; Amman, M. *Environ. Sci. Technol.* **2001**, *35*, 2191−2199.

(5) Lu're, B. A.; Mikhno A. V. *Kinet. Catal.* **1997**, *38*, 490−497.

(6) Pöschl, U.; Letzel, T.; Schauer, C.; Niessner, R. *J. Phys. Chem. A* **2001**, *105*, 4029−4041. Schauer, C.; Niessner, R.; Pöschl, U. Poster presented at the CMD-44 at the Eurotrac-2 2002 Symposium, Garmisch-Partenkierchen, Germany, 2002.

(7) Kamm, S.; Mohler, O.; Naumann, K.-H.; Saathoff, H.; Schurath, U. *Atmos. Environ.* **1999**, *33*, 4651−4661.

(8) Amman, M.; Arens, F.; Gutzwiller, L.; Rössler, E.; Gäggeler, H. W. *EC/Eurotrac-2 Joint Workshop Proceedings*; Ford Research Centre: Aachen, Germany, 1999; pp 236−239.

(9) Atkinson, R.; Arey, J. *Environ. Health Perspect.* **1994**, *102* (Suppl. 4), 117−126.

(10) Pitts, J. N., Jr.; Lokensgard, D. M.; Ripley, P. S.; van Cauwenberghe, K. A.; van Vaeck, L.; Schaffer, S. D.; Thill, A. J.; Belser, W. L. *Science* **1980**, *210*, 1347−1349.

(11) Becker, K. H.; Barnes, I.; Ruppert, L.; Wiesen, P. In *Free Radicals in Biology and Environment*; Minisci, F., Ed.; Kluwer Academic Publishers: Dordrecht, The Netherlands, 1997; Chapter 27, pp 365−385 and references therein.

(12) Güsten, H. In *Free Radicals in Biology and Environment*; Minisci, F., Ed.; Kluwer Academic Publishers: Dordrecht, The Netherlands, 1997; Chapter 28, pp 387−408.

(13) Grosjean, D. *Sci. Total Environ.* **1991**, *100*, 367−414.

(14) Atkinson, R. In *Active Oxygen in Chemistry*; Valentine, J. S., Foote, C. S., Greenberg, A., Liebman, J. F., Eds.; Blackie Academic and Professional: London, 1995; Chapter 7.

(15) Wayne, R. P. *Chemistry of Atmospheres*; Clarendon Press: Oxford, 1996; pp 252−263.

(16) Atkinson, R.; Lloyd, A. *J. Phys. Chem. Ref. Data* **1984**, *13*, 315.

(17) Atkinson, R.; Aschmann, S. M. *Int. J. Chem. Kinet.* **1994**, *26*, 929.
(18) Ghigo, G.; Tonachini, G. *J. Am. Chem. Soc.* **1998**, *120*, 6753−6757. Ghigo, G.; Tonachini, G. *J. Am. Chem. Soc.* **1999**, *121*, 8366−8372. Ghigo, G.; Tonachini, G. *J. Chem. Phys.* **1999**, *109*, 7298−7304. Motta, F.; Ghigo, G.; Tonachini, G. *J. Phys. Chem. A* **2002**, *106*, 4411−4422.
(19) Lee, K. H.; Causà, M.; Park, S. S. *J. Phys. Chem. A* **1998**, *102*, 6020−6024.
(20) Chen, N.; Yang, R. T. *Carbon* **1998**, *36*, 1061−1070.
(21) Kiotani, T.; Tomita, A. *J. Phys. Chem. B* **1999**, *103*, 3434−3441.
(22) Petzold, A.; Stein, C.; Nyeki, S.; Gysel, M.; Weingartner, E.; Baltensperger, U.; Giebl, H.; Hitzenberger, R.; Dopelheuer, A.; Vrchoticky, S.; Puxbaum, H.; Johnson, M.; Hurley, C. D.; Marsh, R.; Wilson, C. W. *Geophys. Res. Lett.* **2002**, *30*, 1719−1722. Grothe, H.; Muckenhuber, H. Presented at the Third Informal Conference on Reaction Kinetics and Atmospheric Chemistry, Helsingør, Denmark, 2002.
(23) Pople, J. A.; Gill, P. M. W.; Johnson, B. G. *Chem. Phys. Lett.* **1992**, *199*, 557−560. Schlegel, H. B. In *Computational Theoretical Organic Chemistry*; Csizsmadia, I. G., Daudel, R., Eds.; Reidel: Dordrecht, The Netherlands, 1981; pp 129−159. Schlegel, H. B. *J. Chem. Phys.* **1982**, *77*, 3676−3681. Schlegel, H. B.; Binkley, J. S.; Pople, J. A. *J. Chem. Phys.* **1984**, *80*, 1976−1981. Schlegel, H. B. *J. Comput. Chem.* **1982**, *3*, 214−218.
(24) Parr, R. G.; Yang, W. *Density Functional Theory of Atoms and Molecules*; Oxford University Press: New York, 1989; Chapter 3. Becke, A. D. *Phys. Rev. A* **1988**, *38*, 3098−3100. Becke, A. D. *ACS Symp. Ser.* **1989**, *394*, 165. Pople, J. A.; Gill, P. M. W.; Johnson, B. G. *Chem. Phys. Lett.* **1992**, *199*, 557−560. Becke, A. D. *J. Chem. Phys.* **1993**, *98*, 5648−5652. Lee, C.; Yang, W.; Parr, R. G. *Phys. Rev. B* **1988**, *37*, 785−789.
(25) Hehre, W. J.; Ditchfield, R.; Pople, J. A. *J. Chem. Phys.* **1972**, *56*, 2257−2261. Hariharan, P. C.; Pople, J. A. *Theor. Chim. Acta* **1973**, *28*, 213−222. Diffuse functions: Clark, T.; Chandrasekhar, J.; Schleyer, P. v. R. *J. Comput. Chem.* **1983**, *4*, 294−301. Multiple polarization functions: Frisch, M. J.; Pople, J. A.; Binkley, J. S. *J. Chem. Phys.* **1984**, *80*, 3265−3269.
(26) Gordon, M. J.; Binkley, J. S.; Pople, J. A.; Pietro, W. J.; Hehre, W. J. *J. Am. Chem. Soc.* **1982**, *104*, 2797. Pietro, W. J.; Francl, M. M.; Hehre, W. J.; Defrees, D. J.; Pople, J. A.; Binkley, J. S. *J. Am. Chem. Soc.* **1982**, *104*, 5039.
(27) Pisani, C.; Dovesi, R.; Roetti, C. *Hartree−Fock Ab Initio Treatment of Crystalline Systems. Lecture Notes in Chemistry*; Springer-Verlag, Heidelberg, 1988; Vol. 48.
(28) Frisch, M. J.; Trucks, G. W.; Schlegel, H. B.; Scuseria, G. E.; Robb, M. A.; Cheeseman, J. R.; Zakrzewski, V. G.; Montgomery, J. A., Jr.; Stratmann, R. E.; Burant, J. C.; Dapprich, S.; Millam, J. M.; Daniels, A. D.; Kudin, K. N.; Strain, M. C.; Farkas, O.; Tomasi, J.; Barone, V.; Cossi, M.; Cammi, R.; Mennucci, B.; Pomelli, C.; Adamo, C.; Clifford, S.; Ochterski, J.; Petersson, G. A.; Ayala, P. Y.; Cui, Q.; Morokuma, K.; Malick, D. K.; Rabuck, A. D.; Raghavachari, K.; Foresman, J. B.; Cioslowski, J.; Ortiz, J. V.; Stefanov, B. B.; Liu, G.; Liashenko, A.; Piskorz, P.; Komaromi, I.; Gomperts, R.; Martin, R. L.; Fox, D. J.; Keith, T.; Al-Laham, M. A.; Peng, C. Y.; Nanayakkara, A.; Gonzalez, C.; Challacombe, M.; Gill, P. M. W.; Johnson, B. G.; Chen, W.; Wong, M. W.; Andres, J. L.; Head-Gordon, M.; Replogle, E. S.; Pople, J. A. *Gaussian 98*, revision A.6; Gaussian, Inc.: Pittsburgh, PA, 1998.
(29) Saunders, V. R.; Dovesi, R.; Roetti, C.; Causà, M.; Harrison, N. M.; Zicovich-Wilson, C. M.; *CRYSTAL'98. User Manual*. Turin University: Turin, Italy, 1999.
(30) Dovesi, R.; Pisani, C.; Roetti, C.; Saunders, V. R. *Phys. Rev. B* **1983**, *28*, 5781−5792.
(31) Causà, M.; Dovesi, R.; Orlando, R.; Pisani, C.; Saunders, V. R. *J. Phys. Chem.* **1988**, *92*, 909−913.
(32) Zicovich-Wilson, C. M.; Dovesi, R. *Int. J. Quantum Chem.* **1998**, *67*, 299−309.
(33) Doll, K.; Harrison, N. M.; Saunders, V. R. *Int. J. Quantum Chem.* **2001**, *82*, 1−12. Doll, K. *Comput. Phys. Commun.* **2001**, *137*, 74−82. Civalleri, B.; D'Arco, Ph.; Orlando, R.; Saunders, V. R.; Dovesi, R. *Chem. Phys. Lett.* **2001**, *348*, 131−138.
(34) Pisani, C.; Causà, M.; Dovesi, R.; Roetti, C. *Prog. Surf. Sci.* **1987**, *25*, 119−137.
(35) Kristyan, S.; Pulay, P. *Chem. Phys. Lett.* **1994**, *229*, 175−180. Perez-Jorda, J. M.; Becke, A. D. *Chem. Phys. Lett.* **1995**, *233*, 134−137. Meijer, E. J.; Sprik, M. *J. Chem. Phys.* **1996**, *105*, 8684−8689. Tsuzuki, S.; Lüthi, H. P. *J. Chem. Phys.* **2001**, *114*, 3949−3957. See, also, for a DFT approach not based on the Kohn−Sham equations: Tran, F.; Weber, J.; Wesołowski, T. A. *Helv. Chim. Acta* **2001**, *84*, 1489−1503. For the use of Møller−Plesset methods to model the interlayer interactions in graphite: Ruuska, H.; Pakkanen, T. A. *J. Phys. Chem. B* **2001**, *105*, 9541−9547.
(36) Pilling, M. J.; Seakins, P. W. *Reaction Kinetics*; Oxford Science Publications: Oxford, 1995; pp 241−251.
(37) The adsorption of a hydrogen atom in a bridged position at 1.3 Å above the midpoint of a C−C bond corresponds to a first-order saddle point. This TS connects two stable minima in which the hydrogen is just above one carbon atom, and its energy locates it 45 kcal mol^{-1} above them. The absorption of a hydrogen atom positioned above the center of one hexagon does not take place, since with this arrangement the two moieties just dissociate. These results can be a first indication of a modest mobility of the radical adsorbates on the graphite surface.
(38) Lu, L.-H.; Sun, K.-C.; Chen, C. *Int. J. Quantum Chem.* **1998**, *67*, 187−197.
(39) Guo, T.; Scuseria, G. E. *Chem. Phys. Lett.* **1991**, *191*, 527−532.
(40) Ghigo, G.; Causà, M.; Maranzana, A.; Tonachini, G. Theoretical Mechanistic Study on the Nitration of Benzene and Naphthalene under Tropospheric and Combustion Conditions. Manuscript to be submitted.
(41) Paredes, J. I.; Martinez-Alonso, A.; Tascon, J. M. D. *Carbon* **2000**, *38*, 1183. Myrick, M. L.; Hud, N. V.; Angel, S. M.; Garvis, D. G. *Chem. Phys. Lett.* **1991**, *180*, 156.
(42) Singer, L. S.; Lewis, L. C. *Appl. Spectrosc.* **1982**, *36*, 52.
(43) Richter, H.; Mazyar, O. A.; Sumathi, R.; Green, W. H.; Howard, J. B.; Bozzelli, J. W. *J. Phys. Chem. A* **2002**, *106*, 4411−4422.
(44) Cioslowski, J.; Liu, G.; Martinov, M.; Piskorz, P.; Moncrieff, D. *J. Am. Chem. Soc.* **1996**, *118*, 5261−5264.
(45) Tyutyulkov, N.; Madjarova, G.; Dietz, F.; Muller, K. *J. Phys. Chem. B* **1998**, *102*, 10183.